ISSN 0015-4628, Fluid Dynamics, 2022, Vol. 57, Suppl. 1, pp. S1–S12. © Pleiades Publishing, Ltd., 2022.

On the Influence of a Spatial Mesh Structure on the Results of Numerical Simulation of a Shock Wave in a Flow around a 3D Model

I. A. Shirokov[a,*] **and T. G. Elizarova**[b]

[a] *Faculty of Computational Mathematics and Cybernetics, Moscow State University, Moscow, 119991 Russia*

[b] *Keldysh Institute of Applied Mathematics, Moscow, 125047, Russia*

** e-mail: ivanshirokov@inbox.ru*

Received June 26, 2019; revised July 18, 2022; accepted July 18, 2022

Abstract—The influence of the structure of a 3D spatial mesh on the quality of numerical modeling of viscous compressible gas flow at a Mach number equal to 3 around a forward-facing part of a rectangular cylinder is demonstrated. The results obtained show that the mesh structure critically affects the shape and the intensity of the head shock wave, and its influence can exceed that of other mesh-related effects. The calculations are performed using a finite volume method implemented for regularized or quasi-gas dynamic equations.

Keywords: shock wave modeling, quasi-gas-dynamic algorithm, mesh structure

DOI: 10.1134/S0015462822601474

1. INTRODUCTION

The accuracy of the numerical solution of the problems of aerodynamics of supersonic flow around models is of paramount importance for designing and studying the flight characteristics of real aircraft. The accuracy of numerical algorithms depends on many factors. The most important among them, the order of accuracy of the difference scheme itself, both in time and space, and the structure of artificial additive and limiting factors that ensure its monotonic behavior, the number of spatial nodes of the difference mesh, and, finally, the structure of the mesh itself.

For numerical simulation of the flow around vehicles with a complex structure, complex multicomponent unstructured meshes must be used, which include tetrahedral meshes. The quality of the calculation as a whole, apart from the characteristics of the difference algorithm, is largely determined by the quality of the spatial mesh employed. The efforts required for creating high-quality meshes can be comparable to those of the entire calculation as a whole, and the problem of constructing "good" spatial meshes becomes of paramount importance [1, 3].

In this study we use the example of the classical problem of an external three-dimensional supersonic flow moving around the end part of a parallelepiped to show the role of a spatial mesh and its influence on the accuracy of bow shock wave modeling in solving the complete Navier–Stokes equations for large Reynolds numbers. An algorithm based on using regularized or quasi-gas-dynamic (QGD) equations is employed as a numerical solution method.

2. DESCRIPTION OF THE PROBLEM

We consider a model in the form of a rectangular parallelepiped the transverse dimensions of which in the Cartesian coordinate system are defined as $-0.015 < y < 0.015$, $-0.015 < z < 0.015$ (here and below, the dimensions are specified in meters). The model is located with a zero angle of attack with respect to the oncoming flow. The computational domain is a rectangular parallelepiped, inside which the model is located in the oncoming air flow directed along the x-axis. The oncoming flow parameters are: gas constant $R = 287$ J/(kg K), adiabatic index $\gamma = 1.4$, Prandtl number $Pr = 14/19$, and the intermolecular interaction index $\omega = 0.74$. The Mach number $Ma = 3$ is considered. The Reynolds number, reduced to 1 m, is $Re = 4.7 \times 10^7$.

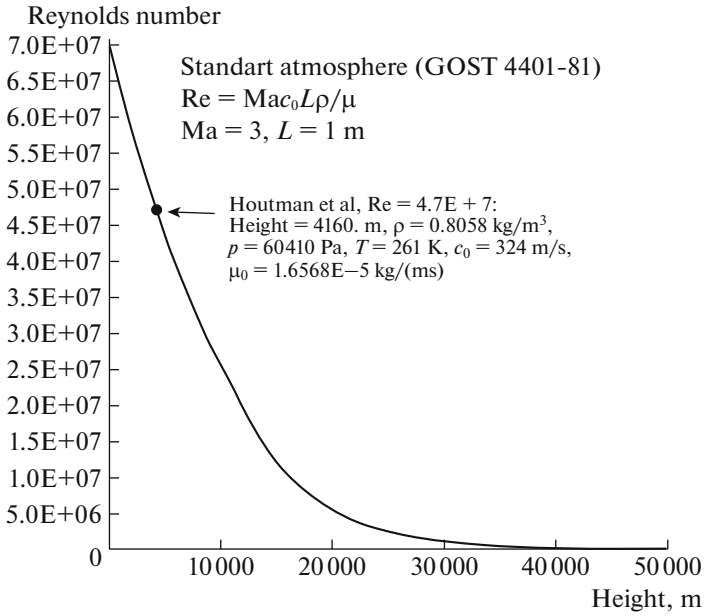

Fig. 1. Reynolds number as a function of flight altitude.

In [4], the external flow moving around an axisymmetric body is studied experimentally and numerically. The results in this study are of great interest as reference data that can be used in the development and testing of numerical methods designed to simulate gas-dynamic flows. In this regard, the dimensions of the model and the dimensionless parameters of the oncoming flow used in this work, which are presented in the previous paragraph, are chosen the same as in [4].

To determine the dimensional parameters of the oncoming flow, we use the data of the standard atmosphere. The model under consideration moves in the atmosphere at a certain altitude. Then, for a given Mach number and a given characteristic size, the dependence of the Reynolds number on the flight altitude in the atmosphere can be determined using the data on the standard atmosphere (GOST 4401-81). Figure 1 shows such a dependence on the flight altitude for Ma = 3. Since the dependence shown is monotonic, the flight altitude is uniquely determined. Knowing the altitude, the dimensional parameters of the oncoming flow in the standard atmosphere can be determined.

The oncoming flow parameters obtained by the described method have the following values: flight altitude 4160 m, density $\rho_0 = 0.8058$ kg/m^3, pressure $p_0 = 60410$ Pa, temperature $T_0 = 261$ K, speed of sound $c_0 = 324$ m/s, and the dynamic viscosity coefficient $\mu_0 = 1.6568 \times 10^{-5}$ kg/(m s).

3. MATHEMATICAL MODEL

As a method for the numerical solution of macroscopic equations of gas dynamics, an algorithm based on the use of regularized or QGD equations is used. The method for constructing these equations and their application to aerodynamic problems are described, in particular, in [5–10]. This system can be considered as a regularized form of the Navier–Stokes (NS) system of equations, which is obtained by a natural procedure of averaging the original system of gas dynamics equations over a small space-time interval. This procedure, which leads to smoothing (regularization) of the original system of equations, is manifested in the emergence in it of additions proportional to a small parameter with the dimension of time. The latter makes it possible to use finite-volume algorithms for their numerical implementation with the approximation of all flow quantities by central differences without resorting to using limiters to ensure their monotonic behavior and conditional stability.

Thus, the difference schemes constructed on the basis of QGD equations have a number of analogies with the Godunov schemes the main advantages of which are [11]: the homogeneity and clarity of the numerical algorithm, the monotonicity of the solution, and the fulfillment of the law of non-decreasing total entropy, along with the capacity to model discontinuous solutions. The main disadvantage of this approach is its first order of accuracy in space. There are a number of studies devoted to enhancing the

accuracy of Godunov's schemes, but if the order of accuracy in space is increased, the fulfillment of the condition of non-decreasing total entropy is no longer ensured. This circumstance, in turn, can lead to the emergence of non-physical solutions of the Euler equations. In particular, it was shown in [11] that, depending on the magnitude of the scheme viscosity and initial conditions, both conventionally known stationary flow patterns and nonphysical non-stationary patterns containing oblique shock waves can be formed. In nature, such solutions are rejected due to the presence of viscous effects, which are necessarily present in the flow. In contrast to Godunov's schemes, no enhancement of the accuracy of QGD schemes was carried out, and no such unphysical flow patterns were observed in the QGD-based approach.

In Cartesian coordinates, in the absence of external forces and heat sources, the QGD system can be represented as [6]

$$\frac{\partial}{\partial t}\rho + \nabla_i j_m^i = 0, \tag{3.1}$$

$$\frac{\partial}{\partial t}\rho u^j + \nabla_i (j_m^i u^j) + \nabla^j p = \nabla_i \Pi^{ij}, \tag{3.2}$$

$$\frac{\partial}{\partial t}E + \nabla_i (j_m^i H) + \nabla_i q^i = \nabla_i (\Pi^{ij} u_j). \tag{3.3}$$

Here, ρ is the gas density; u^i are components of its macroscopic speed; and p is pressure. The total energy of the unit volume E and the total specific enthalpy H of an ideal polytropic gas with adiabatic exponent γ are calculated using formulas

$$E = \frac{\rho u^2}{2} + \frac{p}{\gamma - 1}, \quad H = \frac{E + p}{\rho}. \tag{3.4}$$

The vector of mass flow density j_m^i is defined as

$$j_m^i = \rho(u^i - w^i), \quad w^i = \frac{\tau}{\rho}(\nabla_j \rho u^i u^j + \nabla^i p). \tag{3.5}$$

Viscous stress tensor Π^{ij} and thermal flux q^i are represented as

$$\Pi^{ij} = \Pi_{\text{NS}}^{ij} + \tau u^i \rho \left(u_k \nabla^k u^j + \frac{1}{\rho}\nabla_j p \right) + \tau \delta^{ij} (u_k \nabla^k p + \gamma p \nabla^k u_k), \tag{3.6}$$

$$\Pi_{\text{NS}}^{ij} = \mu \left(\nabla^i u^j + \nabla^j u^i - \frac{2}{3}\nabla^k u_k \right) + \varsigma \delta^{ij} \nabla^k u_k, \tag{3.7}$$

$$q^i = q_{\text{NS}}^i - \tau u^i \rho \left(u_j \nabla^j \varepsilon + p u_j \nabla^j \frac{1}{\rho} \right) \quad q_{\text{NS}}^i = -\kappa \nabla^i T. \tag{3.8}$$

Here, $\varepsilon = p/\rho(\gamma - 1)$ is the internal energy per unit mass; Π_{NS}^{ij} and q_{NS}^i is the viscous stress tensor and thermal flux in the NS system; μ, ς, and κ is the coefficient of shear and bulk viscosity and thermal conductivity, respectively; and T is the gas temperature. Shear viscosity coefficient μ is determined using temperature dependence [6]

$$\mu = \mu_0 \left(\frac{T}{T_0} \right)^{\omega}, \tag{3.9}$$

where μ_0 is the viscosity of gas at temperature T_0, and $0 < \omega < 1$ is the index of intermolecular interaction. The thermal conductivity coefficient is calculated as

$$\kappa = \frac{\mu}{\text{Pr}(\gamma - 1)}. \tag{3.10}$$

Coefficient τ, which controls additional dissipation in the QGD algorithm for a polytropic gas is of the order of the characteristic time between collisions of gas particles [5–7]. Its value is related to the shear viscosity coefficient. To ensure stability of the QGD algorithm in simulating supersonic flows of dense gases, the formula for τ is modified by including into it an additive term that depends on the spatial mesh step and local parameters of the flow

$$\tau = \frac{\mu}{p\mathrm{Sc}} + \frac{\alpha h}{c}, \tag{3.11}$$

where h is the characteristic size of the spatial mesh; c is the local speed of sound; α is an adjusting parameter, which in most cases is assumed to be a constant of the order of 1; and Sc is the Schmidt number, which for gases is close to one [5–7].

The bulk viscosity coefficient can be calculated using an approximating formula [6], in which an ad hoc term is introduced to stabilize the numerical algorithm, so the formula for the bulk viscosity coefficient is presented as

$$\varsigma = \mu\left(\frac{5}{3} - \gamma\right) + \delta\left(\frac{h}{c}\right)p. \tag{3.12}$$

The value of the regularizing additive term here is also determined by local parameters and depends on setting coefficient δ. This introduction of artificial dissipation in QGD equations was used for the first time in [9, 10].

4. REALIZATION OF THE QGD ALGORITHM

To examine the influence of cell shape on simulation results four computational meshes were used: regular uniform *(1)*, regular nonuniform *(2)*, irregular tetrahedral *(3)*, and regular nonuniform with condensation *(4)*.

Uniform mesh *(1)* has cubic cells with a side of 1 mm. The computational area is set then as $-0.07 < y < 0.07$, $-0.07 < z < 0.07$, $-0.05 < x < 0.04$ (dimensions are presented here and below in meters unless stated otherwise). The total number of regular mesh *(1)* nodes is 1 855 088.

The cells of nonuniform mesh *(2)* have the shape of rectangular parallelepipeds. On the surface of the model, the step of the cells is 1 mm as in mesh *(1)*. As the distance from the surface along each axis increases, the mesh step increases in proportion to $\left(1 - \cos\left(l/l_0\right)\right)$, where l is the distance from the surface of the model to the current cell, and l_0 is the distance from the surface of the model to the boundary of the computational area in the case of mesh *(1)*. The computational area is set in this case as $-0.1 < y < 0.1$, $-0.1 < z < 0.1$, $-0.075 < x < 0.04$. The nonuniform mesh remains symmetric with respect to planes $y = 0$ and $z = 0$. The total number of nonuniform mesh *(2)* nodes is 363 888.

Irregular tetrahedral mesh *(3)* was built using the TetGen library [12]. The geometry of the model and the computational area are described in a .poly format file. After the poly-file has been constructed, the mesh is generated using the tetgen.exe -pq1.4/17a0.00007Y command, and the mesh on the surface of the model specified in the poly-file is used as a basis for constructing surface faces of tetrahedral cells. These faces are identical equal-sided right triangles with a leg length of 0.5 mm. The computational area is specified as $-0.07 < y < 0.07$, $-0.07 < z < 0.07$, $-0.05 < x < 0.18$. In this case the model, which is fully contained within the computational area, is set as $-0.015 < y < 0.015$, $-0.015 < z < 0.015$, $0 < x < 0.127$. The total number of irregular mesh nodes is 153 126, and the number of tetrahedral elements is 768 152.

The cells of nonuniform mesh *(4)* are rectangular parallelepipeds as in *(2)*, and it is constructed similar to *(2)* the only difference being that the size of the cells on the face end of the model is 0.3 mm along the x-axis, while on the side surface of the model, it is 0.4 mm along the direction perpendicular to the side surface. The size of other sides of near-wall cells remains equal to 1 mm. The computational area is set in this case as $-0.1 < y < 0.1$, $-0.079 < z < 0.079$, $-0.043 < x < 0.04$, and the mesh remains symmetric with respect to planes $y = 0$ and $z = 0$. The total number of nodes in mesh *(4)* is, similar to mesh *(1)*, 1 855 088.

On uniform meshes *(1), (2),* and *(4)* the QGD equations are approximated by central differences. On uniform mesh *(1)* the accuracy of approximation is of the second order, while in the case of nonuniform meshes, it is of the first order. It should be noted that in the latter case the spatial step in Eqs. (3.11) and (3.12) is constant and equal to the minimal value on the mesh.

For calculation on irregular tetrahedral mesh *(3)* an advanced software package [13] is used, which enables calculations of nonstationary viscous hydrodynamic flows for bodies of any shape. The values of gas-dynamic parameters are set in mesh nodes. The values of gas-dynamic parameters at the computational-area points located between mesh nodes are found as arithmetic mean of values in the nodes. The finite-difference approximation of macroscopic QGD equations is constructed using the control-volume method. The barycentric control volume is built around each mesh node.

Inasmuch as dissipative coefficients (3.11) and (3.12) depend on local parameters, the algorithm provides the tetrahedral mesh with the first order in spatial approximation accuracy.

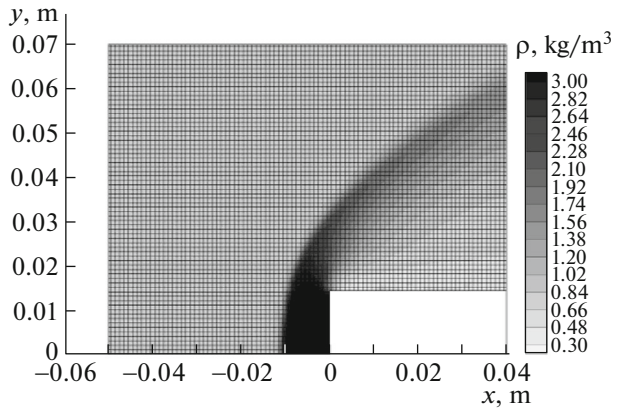

Fig. 2. Uniform mesh (*1*).

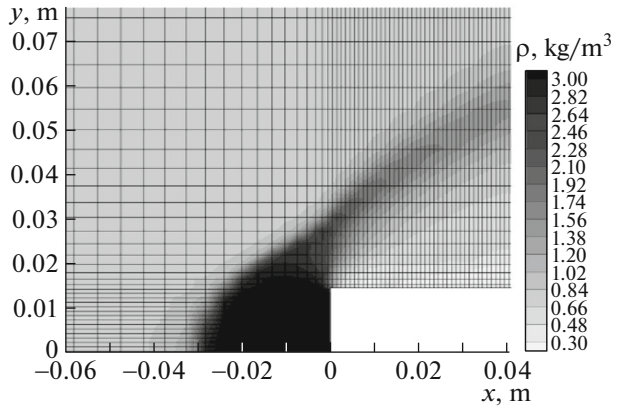

Fig. 3. Nonuniform mesh (*2*).

For all meshes, the solution of the initial boundary value problem for the mesh-based analogs of QGD equations is found using the finite-difference scheme explicitly involving time, which provides the first order of accuracy in time approximation. The calculations were carried out using a K-100 multiprocessor facility [14].

5. SIMULATION RESULTS

Figures 2–5 display the results obtained on uniform mesh *(1)* on the left panel and those obtained on nonuniform mesh *(2)* on the right panel. With the exception of the mesh, all other calculation parameters were the same: $\alpha = 1$; in calculating coefficient δ the following dependence on the local Mach number was used: for $\mathrm{Ma} \geq 2$, $\delta = \delta_1 = 0.5$, for $\mathrm{Ma} \leq 1.5$, $\delta = \delta_2 = 1$, and in the range between Mach numbers 1.5 and 2, coefficient δ linearly increases with the Mach number [8].

Figures 2 and 3 show the computational mesh and density level lines. Figures 4 and 5 display density levels alone to represent more clearly the difference in simulation results.

The use of the uniform mesh (Figs. 2 and 4) makes it possible to obtain a general picture of the flow that is in good agreement with the results of numerical study of a flow around the face end of a cylinder obtained in [6]. The shock wave front, which is well resolved, spans 3–4 mesh cells. In the case of the nonuniform mesh, as Figs. 3 and 5 show, the region of the shock wave front is heavily distorted compared with Figs. 2 and 4. The bow chock front is extended along the line of mesh cell extension (the x-axis) but spans 4 cells as in the case of the uniform mesh.

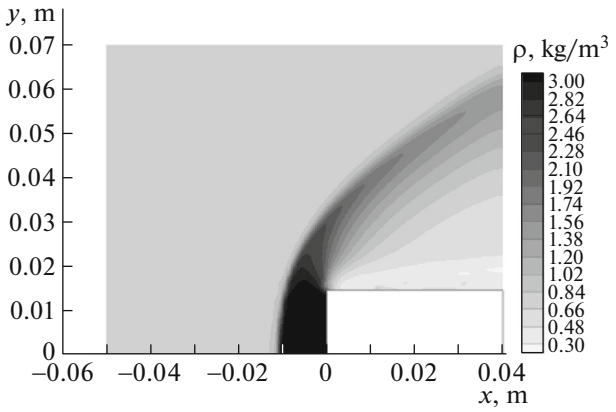

Fig. 4. Uniform mesh (*1*).

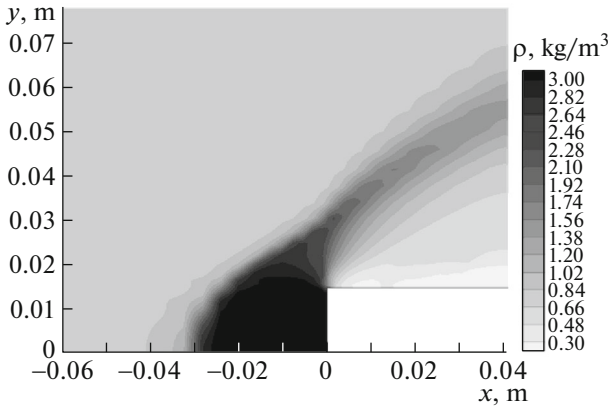

Fig. 5. Nonuniform mesh (*2*).

It should be noted that despite the presence of a distorted and highly elongated shock wave front (see Figs. 3 and 5), in contrast to the Kolgan scheme [11], calculations based on the QGD algorithm does not yield nonstationary flow modes with the occurrence of inclined shock waves.

Stretching of mesh cells along the y-axis (upper part of the image) also results in a deformation of the front of the moving away shock wave albeit in a smaller degree since the intensity of the shock wave is in this region lower.

Near the side surface of the model (in the vicinity of $x = 0.03$ m, $y = 0.03$ m, where the flow velocity is not large) the nonuniform mesh weakly distorts the simulation results compared with the shock wave region.

Figures 6–9 display the results obtained on regular uniform mesh *(1)*, left panel, and on irregular tetrahedral mesh *(3)*, right panel. The calculation parameters are the same and have the same values as in calculations presented in Figs. 2–5, with the following difference: the artificial viscosity coefficients are $\delta_1 = 2$ and $\delta_2 = 5$, i.e., are larger than in the previous case.

Figures 6 and 7 show the computational mesh and the density level lines, while Figs. 8 and 9 display density levels alone.

The results on uniform mesh (*1*) with an increased viscosity also represent the general picture of the flow quite well and, on the whole, reasonably resolve the shock wave front. In this case, the shock wave is somewhat expanded in comparison with Fig. 2, and the shock wave front spans 8 grid cells. In the case of an irregular tetrahedral mesh, as seen in Figs. 7 and 9, the area of the shock wave front is noticeably expanded in comparison with Figs. 6 and 8.

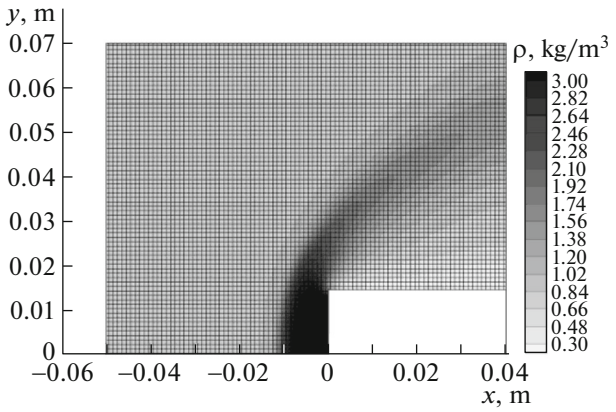

Fig. 6. Uniform mesh (*1*).

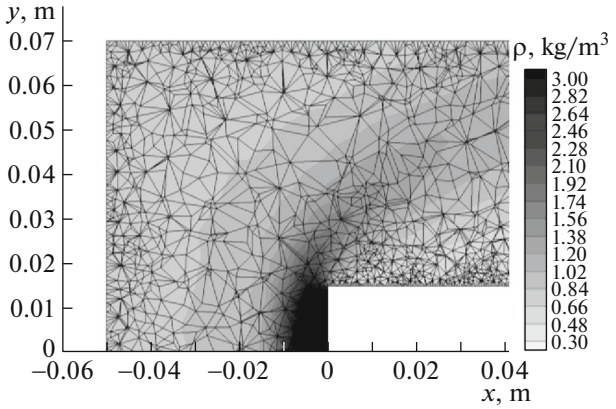

Fig. 7. Irregular mesh (*3*).

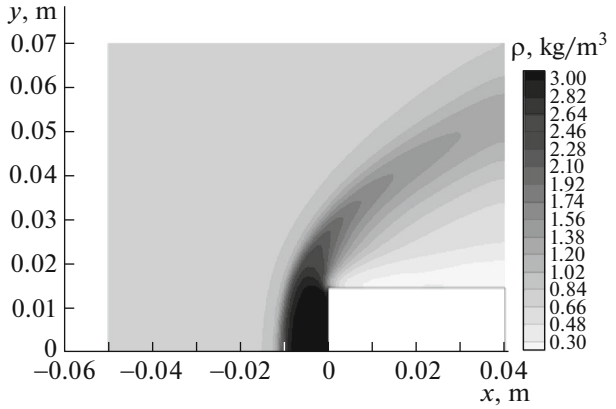

Fig. 8. Uniform mesh (*1*).

To study the influence of various methods of introducing artificial viscosity on the resolution of shock waves, we present the calculation result for the artificial viscosity introduced in the following way. The coefficient of additional dissipation in the QGD algorithm is calculated as

$$\tau = \mu_0 \frac{(T/T_0)^{\omega}}{p\mathrm{Sc}} + \frac{\alpha h}{c}, \tag{5.1}$$

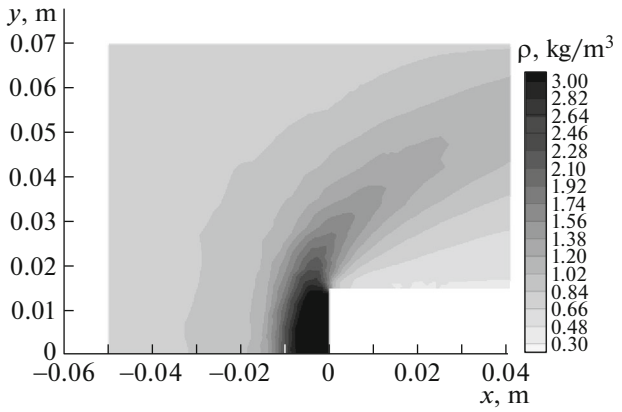

Fig. 9. Irregular mesh (*3*).

where notations are the same as in Eqs. (3.9)–(3.12). Shear viscosity coefficient μ is defined in terms of the coefficient of additional dissipation

$$\mu = \tau p \mathrm{Sc}, \tag{5.2}$$

the thermal conductivity coefficient is calculated as

$$\kappa = \frac{\mu}{\mathrm{Pr}(\gamma - 1)}, \tag{5.3}$$

and the coefficient of bulk viscosity is defined using approximation formula

$$\varsigma = \mu\left(\frac{5}{3} - \gamma\right) \tag{5.4}$$

Thus, Eqs. (3.9)–(3.12) are replaced by Eqs. (5.1)–(5.4). Such an introduction of artificial viscosity into the QGD algorithm is a standard approach [6], in contrast to the variant with the introduction of artificial viscosity as an additional term in second viscosity (3.12), and its exclusion from molecular viscosity (3.9). In this case, coefficient α alone is the adjusting parameter.

Figure 10 shows the density level lines calculated based on the QGD algorithm with artificial viscosity of form (5.1)–(5.4) using $\alpha = 0.3$ and uniform mesh (*1*). Similar to Figs. 2 and 4, in Fig. 10, the computational mesh is shown on the left, and the density levels alone are shown on the right.

These results are close to those obtained on a uniform mesh with artificial viscosity of form (3.9)–(3.12). It can be concluded that the two considered methods of introducing artificial viscosity are virtually equivalent if the same uniform mesh is used.

To study the effect of mesh condensation near the shock wave region, calculations were carried out on a nonuniform mesh with condensation (*4*). Figure 11 shows the density level lines calculated on the basis of the QGD algorithm with artificial viscosity of form (3.9)–(3.12), the calculation parameters being the same as those corresponding to Figs. 7 and 9.

Similar to Figs. 2 and 4, Fig. 12 shows the computational mesh on the left, and the density levels alone are shown on the right. It can be clearly seen that the mesh condensation area strongly distorts the shape of the shock wave front. In passing through the condensation region boundary, the front undergoes a kink. In addition, in this case, the shock wave is located much closer to the frontal surface of the model than in the case of using uniform and tetrahedral meshes with the same calculation parameters (Figs. 6–9). It should be noted that Lunev's approximation formula [6] for the distance between the shock wave and the end of the cylinder around which the flow moves gives in this case a value of about 0.01 m, which agrees very well with the results on the uniform and tetrahedral meshes and does not agree with the result obtained on the nonuniform mesh with condensation.

We also note that the construction of a mesh with condensation in the shock wave region, even in the considered model case, is a very difficult task, since the shock wave front has a curvilinear shape, and its location is not known in advance. This is all the more true for real problems, for example, for calculating the flow around aircraft of various shapes, around which a complex structure of shock waves is formed, the location of which is not known in advance.

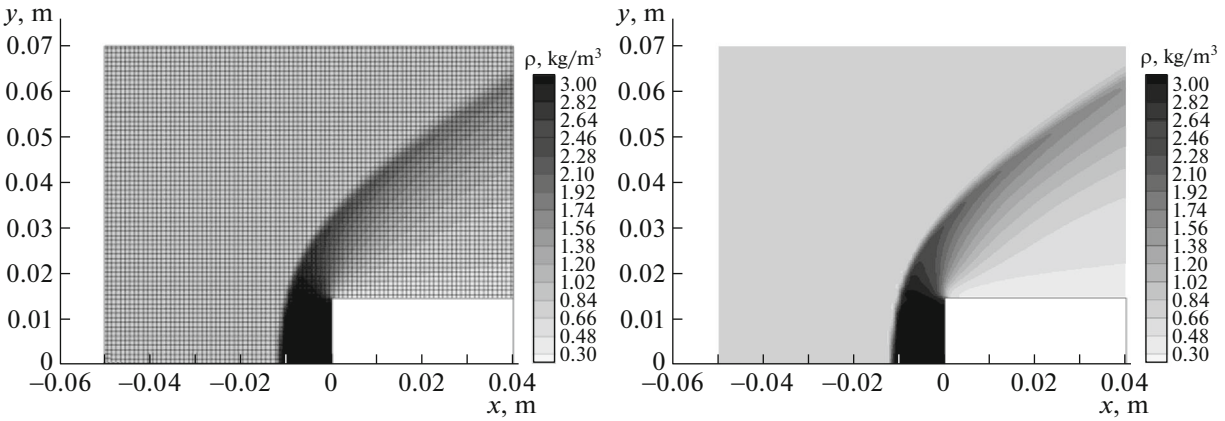

Fig. 10. Uniform mesh (*1*), artificial viscosity introduced according to Eqs. (5.1)–(5.4).

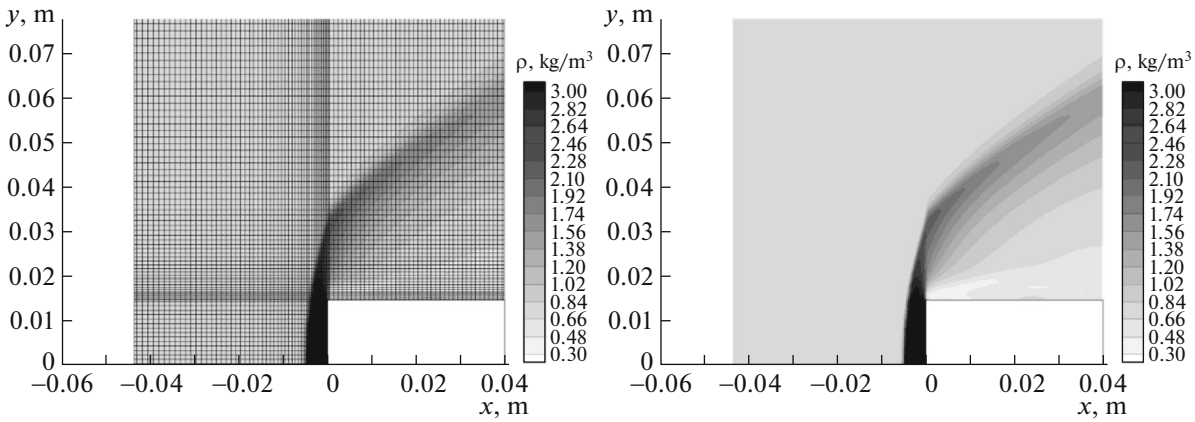

Fig. 11. Nonuniform mesh (*4*), artificial viscosity introduced according to Eqs. (3.9)–(3.12).

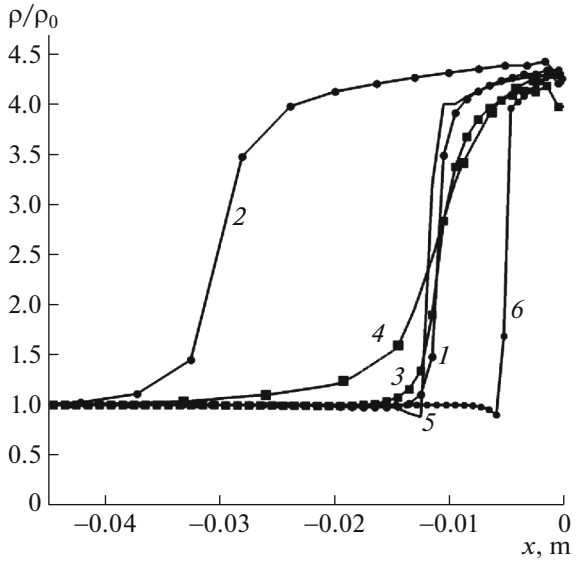

Fig. 12. Density profiles in the bow shock wave.

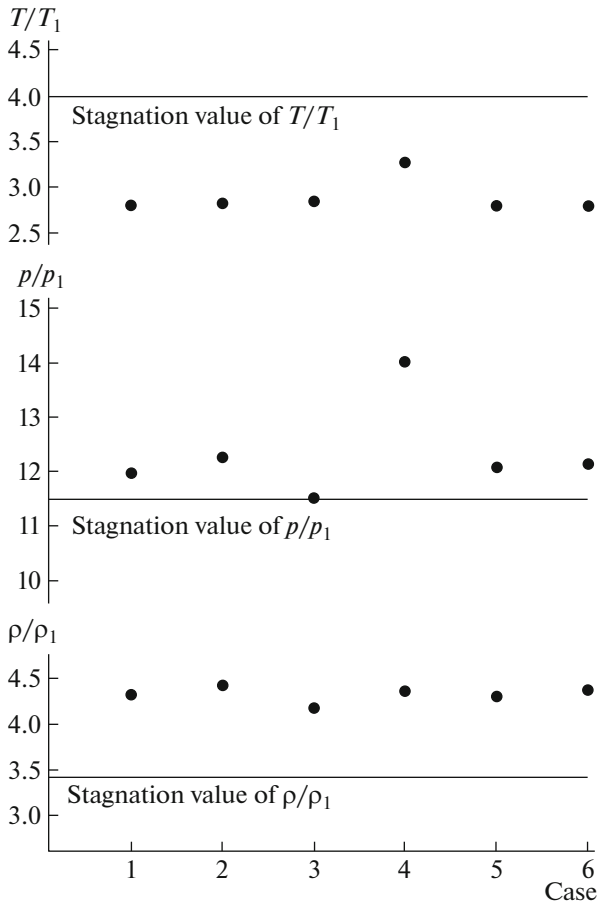

Fig. 13. Maximum values of density and pressure in comparison with stagnation parameters.

As in the case of nonuniform mesh (*2*) (see Figs. 2 and 4), extension of the mesh cells along the y-axis (in the upper right part of the figure) distorts the shape of the shock wave front to a much lesser extent than in the region of the head shock wave.

The resolution of the shock wave front on the mesh can be seen in more detail in Fig. 12, which shows one-dimensional density profiles depending on the distance from the frontal surface of the streamlined body at $y = 0$ and $z = 0$. Markers on profile curves correspond to mesh cell boundaries.

Curves *1*, *3,* and *5* correspond to uniform mesh *(1)*, curve *2*, to nonuniform mesh *(2)*, curve *4*, to irregular tetrahedral mesh *(3)*, and curve *6* corresponds to nonuniform mesh *(4)*. Curves *1* and *2* are obtained for $\delta_1 = 0.5$, $\delta_2 = 1$. Curves *3, 4*, and 6 correspond to $\delta_1 = 2$ and $\delta_2 = 5$. For curves *1*–*4* and 6, coefficient $\alpha = 1$. Curve *5* is obtained using Eqs. (5.1)–(5.4) instead of (3.9)–(3.12) and the coefficient $\alpha = 0.3$.

Comparison of curves *1* and *2* obtained on uniform and nonuniform meshes, other conditions being equal, clearly shows that the head front wave "is stretched" along with mesh cells. A comparison of curves *3* and *4* obtained on uniform and nonuniform meshes, other conditions being equal, shows that in the vicinity of the body around which the flow moves ($x > -0.01$ m) both meshes yield similar results since the irregular mesh if fairly fine. If distance from the surface increases ($x < -0.01$ m) the broadening of the shock wave front is seen in the case the irregular mesh is used (curve *4*). Similar to the case of regular nonuniform mesh the stretching of the shock wave front corresponds to coursing of mesh cells. Curve *6* obtained on nonuniform mesh *(4)* shows a strong shift of the shock wave front to the frontal surface of the model although the shock wave front is resolved very well. If a uniform mesh is used (curves *1*, *3*, and *5*), fairly close results are obtained for various options for introducing artificial viscosity. However, it can be noticed that with a decrease in artificial viscosity, the shock wave front becomes narrower.

An analysis of the results suggests a conclusion that the use of uniform meshes for simulation of shock wave problems is preferable, since it provides the absence of distortion and shift of the shock wave front.

Table 1. Maximum values of density and pressure in comparison with stagnation parameters

	Mesh	Artificial viscosity (equations)	Values of coefficients	$\frac{\rho_{max}}{\rho_0}$	$\frac{p_{max}}{p_0}$	$\frac{T_{max}}{T_0}$
1	Uniform *(1)*	(3.9)–(3.12)	$\alpha = 1$ $\delta_1 = 0.5,\ \delta_2 = 1$	4.33	11.98	2.81
2	Nonuniform *(2)*	(3.9)–(3.12)	$\alpha = 1$ $\delta_1 = 0.5,\ \delta_2 = 1$	4.43	12.27	2.83
3	Uniform *(1)*	(3.9)–(3.12)	$\alpha = 1$ $\delta_1 = 2,\ \delta_2 = 5$	4.18	11.52	2.85
4	Irregular *(3)*	(3.9)–(3.12)	$\alpha = 1$ $\delta_1 = 2,\ \delta_2 = 5$	4.37	14.02	3.28
5	Uniform *(1)*	(5.1)–(5.4)	$\alpha = 3$	4.31	12.08	2.80
6	Nonuniform *(4)*	(3.9)–(3.12)	$\alpha = 1$ $\delta_1 = 2,\ \delta_2 = 5$	4.38	12.14	2.80
	Values of stagnation parameters			3.42	11.49	4.00

To estimate the accuracy of the simulation results in quantitative terms, the table presents a comparison of the normalized maximum values of density and pressure behind the shock wave near the frontal part of the model, depending on the mesh used and the method of introducing artificial dissipation. The number of the variant corresponds to the numbering of the curves in Fig. 12. Theoretical values of the stagnation parameters, which are used as reference values (presented in the last line of the Table 1), are calculated for a non-viscous, non-heat-conducting gas based on the Rankine–Hugoniot conditions and the Bernoulli theorem [6].

The same data is shown in Fig. 13, where the abscissa shows the numbers of options corresponding to Table 1. It can be seen that the calculation data obtained on a uniform mesh are generally closer to the theoretical values of the stagnation parameters.

The presented results show that the use of a uniform regular grid in modeling flows including shock waves is preferable, since this choice increases the accuracy of modeling and the resolution of fronts.

6. CONCLUSIONS

The study shows the influence of the structure of a 3D spatial mesh on the quality of numerical solution in the problem of a flow of the viscous compressible gas around the end of a rectangular parallelepiped at the Mach number Ma = 3. The results show that the mesh structure has the determining influence on the shape and intensity of the front shock wave, which may exceed the influence of other mesh-related effects, for example, the value of artificial viscosity and the way it is introduced. The order of accuracy of the difference scheme per se may turn out to be insignificant in calculating discontinuous solutions on heavily nonuniform meshes. Therefore, the issues related to the construction of "quality" meshes for the determining flows around a model acquire paramount importance.

FUNDING

This study was supported by the Russian Science Foundation project no. 19-11-00169.

REFERENCES

1. Zheleznyakova, A.L. and Surzhikov, S.T., Application of the method of splitting by physical processes for the computation of a hypersonic flow over an aircraft model of complex configuration, *High Temp.,* 2013, vol. 51, no. 6, pp. 816–830.
2. Zheleznyakova, A.L. and Surzhikov, S.T., *Na puti k sozdaniyu modeli virtual'nogo GLA. I* (On the Way for Generating Virtual Model of Hypersonic Aircraft. I), Moscow: Institute for Problems in Mechanics, RAS, 2013.

3. Zheleznyakova, A.L. and Surzhikov, S.T., A molecular dynamics-based triangulation of multiple NURBS-surfaces for complex products of the aviation and space-rocket industry, *Fiz.-Khim. Kinet. Gaz. Din.,* 2014, vol. 15, no. 1. http://chemphys.edu.ru/issues/2014-15-1/articles/108/12/.
4. Houtman, E.M., Bannink, W.J., and Timmerman, B.H., Experimental and computational study of a blunt cylinder-flare model in high supersonic flow, *Report no. LR-796,* Delft: Delft Univ. of Technology, 1995.
5. Chetverushkin, B.N., *Kinetic Schemes and Quasi-Gas Dynamic System of Equations,* Barselona: CIMNE. 2008.
6. Elizarova, T.G., *Quasi-Gas Dynamic Equations,* Dordrecht: Springer, 2009.
7. Sheretov, Yu.V., *Regulyarizovannyeuravneniya gidrodinamiki* (Regularized Hydrodynamic Equations), Tver: Tver State Univ., 2016. https://elibrary.ru/item.asp?id=30097584.
8. Elizarova, T.G. and Shirokov, I.A., *Regulyarizovannye uravneniya i primery ikh ispol'zovaniya pri modelirovanii gazodinamicheskikh techenii* (Regularized Equations and Examples of Their Use in the Modeling of Gas-Dynamic Flows), Moscow: MAKSPress, 2017. https://elibrary.ru/item.asp?id=29352202.
9. Shirokov, I.A. and Elizarova, T.G., Computer simulation of the supersonic flow of a viscous compressible gas around a model body on the basis of the quasi-gas-dynamic algorithm, *Fiz.-Khim. Kinet. Gaz. Din.,* 2017, vol. 18, no. 2. http://chemphys.edu.ru/issues/2017-18-2/articles/721.
10. Elizarova, T.G. and Shirokov, I.A., Artificial dissipation coefficients in regularized equations of supersonic aerodynamics, *Dokl. Math.,* 2018, vol. 98, no. 3, pp. 648–651.
11. Tunik, Yu.V., Problems of numerical modelling on the basis of some modifications of the Godunov's scheme, *Fiz.-Khim. Kinet. Gaz. Din.,* 2018, vol. 19, no. 1. http://chemphys.edu.ru/issues/2018-19-1/articles/701/.
12. TetGen: a quality tetrahedral mesh generator. http://tetgen.berlios.de/.
13. Kudryashova, T.A., Polyakov, S.V., and Sverdlin, A.A., Calculation of gas flow parameters around reentry vehicle, *Math. Models Comput. Simul.,* 2008, vol. 1, no. 4, pp. 445–452.
14. K-100 System, Moscow: Keldysh Institute of Applied Mathematics RAS. http://www.kiam.ru/MVS/resourses/k100.htm.

Translated by M. Shmatikov